Supporting Information
for

X-ray absorption spectroscopy quantitative analysis of biomimetic copper(II) complexes with tridentate nitrogen ligands mimicking the tris(imidazole) array of protein centres

Elena Borghi*[a] and Luigi Casella[b]

[a]Dipartimento di Chimica, Università di Roma "La Sapienza", Piazzale A. Moro 5, 00185 Roma, Italy and [b]Dipartimento di Chimica Generale, Università di Pavia, via Taramelli 12, 27100 Pavia, Italy

e.borghi@caspur.it and bioinorg@unipv.it

SI-1. MS XANES simulations

The software procedure, MXAN[1-3], is able to fit the XANES part of the experimental spectra. The method performs the fit between the experimental spectrum and several theoretical calculations obtained by changing a defined set of structural parameters around the absorbing atom. The MXAN method, properly taking into account all the multiple scattering contributions, calculates exactly the total photon absorption cross-section. The absorption coefficient is directly given as a function of the energy, allowing an immediate fit of the experimental data. The optimisation in parameter space is achieved using the MINUIT program of the CERN library by performing the minimisation of the square residual function S^2 defined as:

$$S^2 = n\frac{\sum_{i=1}^{m} w_i\left[\left(y_i^{th} - y_i^{exp}\right)\varepsilon_i^{-1}\right]^2}{\sum_{i=1}^{m} w_i}$$

where n is the number of independent parameters, m is the number of data points, y_i^{th} and y_i^{exp} are the theoretical and experimental values of absorption, respectively, ε_i is the individual error in the experimental data set, and w_i is a statistical weight. For w_i = constant = 1, the square residual function, S^2, becomes the statistical χ^2 function. The estimate of the experimental error represented by ε_i, was considered constant in the fitting procedure, and in this case, it was assumed equal to ~1% of the experimental edge jump. This procedure uses the set of programs developed at the INFN Laboratori Nazionali di Frascati[4] by the Frascati theory group: VGEN, which is a generator of muffin-tin (MT) potentials, the CONTINUUM code for the full multiple scattering cross-section calculation.

The MS calculations are done in the frame of one-electron theory by using a molecular electron potential calculated with the MT approximation. The MT potential is calculated around each atomic species (the MT spheres). The MT radii are chosen according to the Norman criterion, with specified percentage of overlap allowed between the contiguous spheres, and the potential is recalculated at each step of the minimization procedure keeping the overlap factor fixed. The Coulomb part of the potential is calculated using the atomic charge densities of Clementi and Roetti tables.[5] The exchange correlation part of the potential can be calculated using the complex Hedin–Lundqvist (H-L) optical form.[6] To avoid the over damping at low energies of the complex part of the HL potential in the case of covalent molecular systems, MXAN uses a phenomenological approach that takes into account the inelastic processes by a convolution of the theoretical spectrum with a broadening function. This calculation uses only the real part of the HL potential, with a suitable Lorentzian function having an energy-dependent width of the form $\Gamma tot(E) = \Gamma c + \Gamma(E)$. The constant part, Γc, is the energy independent broadening value, includes the core-hole lifetime and the experimental resolution. The energy-dependent term, $\Gamma(E)$, represents all the inelastic processes, accounting for any damping associated with the inelastic losses of the photoelectron in the final state. Both parameters are refined during the fitting procedure. The $\Gamma(E)$ function is zero below an onset energy, Es, (which corresponds to the plasmon excitation energy) and begins to increase from a value, As, (which corresponds to the plasmon excitation amplitude). Their numerical values are derived at each computational step of optimization of the structural parameters (*i.e.*, for each geometric configuration) on the basis of a Monte Carlo fit. The MXAN method introduces four non-structural parameters (*i.e.* Fermi energy, broadening parameters (energy-independent/dependent), overlap between the MT radii). The coordination numbers and the Debye-Waller factors are not treated, the edge jump (normalization) and the edge position (alignment) are unrelated to the fitted structural parameters, so the relevant parameters are essentially geometrical.
The non-structural parameters are refined by Monte Carlo search at each step. In a final minimization cycle to get parameters errors, and to avoid artificial results, they were fixed.

The minimization strategy employed in this study uses as structural parameters the polar coordinates (distances and polar angles) of the first ligands to the absorbing atom, put in the center of the coordinate system. Atoms linked to the first ligands

in the input coordinate file rigidly follow the movements of these ligands without changing the relative position. The only statistical errors that can be calculated numerically by the MIGRAD routine are those on polar parameters of the first-shell donors. In the case of test system, the $[Cu(2\text{-}BB)(N_3)]^+$ cation, the right geometrical configuration has been recovered within an error of the order of 0.03-0.06 Å in the interatomic distances and about 3 degrees in the angle determination. For the $[Cu(2\text{-}BB)(H_2O)_n]^+$ cation in the powdered complex $[Cu(2\text{-}BB)(H_2O)_n](ClO_4)\cdot(H_2O)_{2-n}$ (n=1 or 2) the "true actual" configuration obtained for the two independent best-fitting simulations show an error of the order of 0.02-0.04 Å in bond distances and of 2-3 degrees in the angles. Ligand angles can be added in the input coordinate file, so that the program MXAN will provide automatically their best-fitting values. Furthermore the MXAN procedure supplies as output file the best fitting structure in a format readable by molecule viewer programs. All bond distances and bond angles, different from the first-shell ones, reported in Tables SI-1 1, SI-1 2, SI-1 3 have been evaluated with the Mercury program available from the Cambridge Crystallographic Data Centre.

Table SI-1 1. Comparison of the bond distances (Å) and the bond angles (deg) for the $[Cu(2\text{-}BB)(N_3)](ClO_4)$ crystal (XRD data with statistical errors from ref. 7) and $[Cu(2\text{-}BB)(N_3)](ClO_4)$ powder (MXAN best-fit parameters data). The right geometrical configuration has been recovered within an error of the order of 0.03-0.06 Å in the interatomic distances (**a**) and about 3 degrees in the angle determination (**b**).

Atom 1	Atom 2	XRD Distances	MXAN Distances [a]
Cu	N1	1.962(6)	$1.96_0 \pm 0.03$
Cu	N3	1.959(6)	$1.95_6 \pm 0.03$
Cu	N5	2.003(6)	$2.00_1 \pm 0.03$
Cu	N6	1.946(6)	$2.01_3 \pm 0.06$
N6	N7	1.150(8)	1.148
N7	N8	1.172(9)	1.172
N1	C1	1.335(9)	1.335
N1	C4	1.38(1)	1.387
N2	C1	1.35(1)	1.352
N2	C2	1.48(1)	1.472
N2	C3	1.37(1)	1.378
N3	C9	1.32(1)	1.315
N3	C12	1.39(1)	1.411
N4	C9	1.36(1)	1.362
N4	C10	1.47(1)	1.461
N4	C11	1.37(1)	1.388
N5	C17	1.50(1)	1.488
N5	C19	1.49(1)	1.493
C1	C18	1.49(1)	1.325
C3	C4	1.42(1)	1.414
C3	C5	1.35(1)	1.345
C4	C8	1.39(1)	1.380
C5	C6	1.38(1)	1.382
C6	C7	1.42(1)	1.418
C7	C8	1.37(1)	1.367
C9	C20	1.48(1)	0.974
C11	C12	1.38(1)	1.387
C11	C13	1.41(1)	1.410
C12	C16	1.35(1)	1.357
C13	C14	1.35(1)	1.353
C14	C15	1.41(1)	1.416
C15	C16	1.40(1)	1.404
C17	C18	1.52(1)	1.524
C19	C20	1.53(1)	1.523

Atom 1	Atom 2	Atom 3	XRD Angles	MXAN Angles [b]
N1	Cu	N3	150.5(3)	$150.3_5 \pm$
N1	Cu	N5	95.0(2)	$91.2_4 \pm$
N3	Cu	N5	91.1(3)	$80.8_6 \pm$
N1	Cu	N6	94.0(3)	$102.0_2 \pm$
N3	Cu	N6	98.5(3)	$101.1_4 \pm$
N5	Cu	N6	142.5(3)	$143.5_4 \pm$
Cu	N1	C1	125.7(6)	125.66
Cu	N1	C4	127.5(4)	127.40
Cu	N3	C9	125.7(5)	125.76
Cu	N3	C12	125.8(5)	126.09
Cu	N5	C17	111.7(5)	111.83
Cu	N5	C19	106.2(4)	105.76
Cu	N6	N7	124.6(4)	126.39
N6	N7	N8	176.3(9)	176.04

C1	N1	C4	106.8(6)	106.94
C1	N2	C2	127.3(7)	127.43
C1	N2	C3	109.0(6)	108.94
C2	N2	C3	123.7(7)	123.63
C9	N3	C12	108.1(6)	107.65
C9	N4	C10	126.1(6)	126.22
C9	N4	C11	107.5(6)	107.17
C10	N4	C11	126.3(7)	125.50
C17	N5	C19	111.1(6)	111.18
N1	C1	N2	110.7(7)	110.61
N1	C1	C18	125.2(7)	127.89
N2	C3	C4	104.9(7)	105.13
N2	C3	C5	131.6(7)	131.57
C4	C3	C5	123.4(7)	123.22
N1	C4	C3	108.6(6)	108.33
N1	C4	C8	132.5(/)	132.52
C3	C4	C8	118.8(7)	119.00
C3	C5	C6	117.6(7)	117.70
C5	C6	C7	120.1(9)	120.06
C6	C7	C8	121.4(()	121.41
C4	C8	C7	118.5(7)	118.39
N3	C9	N4	110.6(6)	111.09
N3	C9	C20	127.4(7)	136.32
N4	C9	C20	122.0(7)	99.50
N4	C11	C12	107.3(7)	107.24
N4	C11	C13	132.0(8)	132.09
C12	C11	C13	120.7(7)	120.66
N3	C12	C11	106.5(7)	106.82
N3	C12	C16	130.9(8)	130.56
C11	C12	C16	122.6(7)	122.62
C11	C13	C14	116.7(8)	116.61
C13	C14	C15	122.9(8)	123.31
C14	C15	C16	119.3(8)	118.86
C12	C16	C15	117.8(8)	117.93
N5	C17	C18	119.5(7)	110.41
C1	C18	C17	113.6(6)	113.33
N5	C19	C20	111.1(7)	111.13
C9	C20	C19	113.8(7)	103.11

Table SI-1 2. Bond distances (Å) for the $[Cu(2\text{-}BB)(H_2O)_n]^+$ cation in the non-crystalline complex $[Cu(2\text{-}BB)(H_2O)_n](ClO_4)\cdot(H_2O)_{2-n}$ (n=1 or 2) with five-coordinated Cu(3N)(2O) and four-coordinated Cu(3N)(O) cores derived from MXAN best-fit parameters data. Structures 1 and 2 are related, respectively, to the XRD data of the $[Cu(2\text{-}BB)(MeOH)(ClO_4)]^+$ and the $[Cu(2\text{-}BB)(NO_2)]^+$ cations considered as starting models (*see text*).

		Cu(3N)(2O) core MXAN distances		**Cu(3N)(O) core MXAN distances**		**$[Cu(2\text{-}BB)(H_2O)_n]^+$ MXAN mean distances**	
Atom 1	**Atom 2**	**structure 1**	**structure 2**	**structure 1**	**structure 2**	**Cu(3N)(2O)**	**Cu(3N)(O)**
Cu	Oa	2.116	2.083	2.116	2.083	2.010	2.010
Cu	Ob	2.466	2.509	——	——	2.488	——
Cu	N1	1.944	1.952	1.944	1.953	1.948	1.949
Cu	N3	1.950	1.951	1.949	1.951	1.951	1.950
Cu	N5	2.012	2.003	2.012	2.004	2.008	2.008
N1	C1	1.304	1.338	1.306	1.338	1.321	1.322
N1	C4	1.398	1.383	1.398	1.383	1.391	1.391
N2	C1	1.344	1.386	1.344	1.386	1.365	1.365
N2	C2	1.475	1.468	1.476	1.458	1.472	1.467
N2	C3	1.363	1.359	1.363	1.359	1.361	1.361
N3	C9	1.328	1.320	1.327	1.319	1.324	1.323
N3	C12	1.386	1.425	1.387	1.425	1.406	1.406
N4	C9	1.350	1.339	1.351	1.338	1.345	1.345
N4	C10	1.467	1.467	1.467	1.467	1.467	1.467
N4	C11	1.370	1.395	1.370	1.395	1.383	1.383
N5	C17	1.447	1.514	1.448	1.514	1.481	1.481
N5	C19	1.390	1.530	1.389	1.530	1.460	1.460
C1	C18	1.537	1.382	1.571	1.386	1.460	1.479
C3	C4	1.389	1.413	1.388	1.412	1.401	1.400
C3	C5	1.383	1.413	1.382	1.412	1.398	1.397
C4	C8	1.391	1.382	1.391	1.382	1.387	1.387
C5	C6	1.444	1.359	1.445	1.359	1.402	1.402
C6	C7	1.367	1.419	1.365	1.419	1.393	1.392
C7	C8	1.366	1.403	1.367	1.403	1.385	1.385
C9	C20	1.519	1.688	1.331	1.338	1.604	1.335
C11	C12	1.401	1.403	1.402	1.403	1.402	1.403
C11	C13	1.404	1.374	1.404	1.375	1.389	1.390
C12	C16	1.373	1.371	1.372	1.371	1.372	1.372
C13	C14	1.365	1.348	1.365	1.347	1.357	1.356
C14	C15	1.391	1.415	1.391	1.414	1.403	1.403
C15	C16	1.378	1.390	1.378	1.390	1.384	1.384
C17	C18	1.494	1.513	1.494	1.514	1.504	1.504
C19	C20	1.412	1.536	1.412	1.536	1.474	1.474

Table SI-1 3. Bond angles (deg) for the $[Cu(2\text{-}BB)(H_2O)_n]^+$ cation in the non-crystalline complex $[Cu(2\text{-}BB)(H_2O)_n](ClO_4)\cdot(H_2O)_{2-n}$ (n=1 or 2) with five-coordinated Cu(3N)(2O) and four-coordinated Cu(3N)(O) cores derived from MXAN best-fit parameters data. Structures 1 and 2 are related, respectively, to the XRD data of the $[Cu(2\text{-}BB)(MeOH)(ClO_4)]^+$ and the $[Cu(2\text{-}BB)(NO_2)]^+$ cations considered as starting models (*see text*).

			Cu(3N)(2O) MXAN Angles		**Cu(3N)(O) MXAN Angles**		**$[Cu(2\text{-}BB)(H_2O)_2]^+$ MXAN mean angles**	
Atom 1	**Atom 2**	**Atom 3**	**structure 1**	**structure 2**	**structure 1**	**structure 2**	**Cu(3N)(2O)**	**Cu(3N)(O)**
Oa	Cu	Ob	*146.08*	*65.02*	——	——	*105.55*	——
Oa	Cu	N1	*85.32*	*98.03*	*91.20*	*98.90*	*91.68*	*95.05*
Oa	Cu	N3	*96.63*	*75.03*	*87.83*	*80.06*	*85.83*	*83.95*
Oa	Cu	N5	*86.95*	*141.23*	*99.75*	*137.35*	*114.09*	*118.55*
Ob	Cu	N1	*75.41*	*95.84*	——	——	*85.63*	——
Ob	Cu	N3	*99.33*	*87.05*	——	——	*93.19*	——
Ob	Cu	N5	*122.68*	*76.83*	——	——	*99.76*	——
N1	Cu	N3	172.44	170.57	173.79	172.70	171.51	173.25
N1	Cu	N5	97.62	92.22	96.77	93.97	94.92	95.37
N3	Cu	N5	89.79	97.18	89.44	91.59	93.49	90.52
Cu	N1	C1	124.24	124.81	124.19	124.78	124.53	124.49
Cu	N1	C4	128.50	127.23	128.53	127.20	127.82	127.87
Cu	N3	C9	126.57	127.14	126.60	127.18	126.86	126.89
Cu	N3	C12	125.62	126.57	125.60	126.59	126.10	126.10
Cu	N5	C17	117.20	108.29	117.18	108.27	112.75	112.73
Cu	N5	C19	119.14	111.28	119.15	111.27	115.21	115.21
C1	N1	C4	106.42	107.95	106.42	108.02	107.19	107.22
C1	N2	C2	126.54	124.88	126.51	124.87	125.71	125.69
C1	N2	C3	108.09	108.46	108.12	108.45	108.28	108.29
C2	N2	C3	125.35	126.60	125.35	126.62	125.98	125.99
C9	N3	C12	106.81	105.83	106.81	105.78	106.32	106.30
C9	N4	C10	127.26	126.56	127.29	126.56	126.91	126.925
C9	N4	C11	107.92	108.06	107.90	108..05	107.99	107.98
C10	N4	C11	124.81	125.38	124.80	125.38	125.10	125.09
C17	N5	C19	119.15	107.19	119.19	107.19	113.17	113.19
N1	C1	N2	111.69	109.31	111.62	109.28	110.50	110.45
N1	C1	C18	123.60	128.43	123.11	125.54	126.02	124.33
N2	C1	C18	122.84	119.36	124.30	120.15	121.10	122.23
N2	C3	C4	106.03	106.57	106.04	106.58	106.30	106.31
N2	C3	C5	132.22	131.59	132.18	131.60	131.91	131.89
C4	C3	C5	121.72	121.84	121.76	121.82	121.78	121.79
N1	C4	C3	107.73	107.71	107.77	107.68	107.72	107.73
N1	C4	C8	131.51	131.94	131.45	131.98	131.73	131.72
C3	C4	C8	120.75	120.32	120.76	120.32	120.54	120.54
C3	C5	C6	116.20	116.80	116.18	116.82	116.50	116.50
C5	C6	C7	119.65	122.57	119.63	122.58	121.11	121.11
C6	C7	C8	122.34	120.16	122.35	120.17	121.25	121.26
C4	C8	C7	118.06	118.27	118.02	118.25	118.17	118.14
N3	C9	N4	111.17	112.73	111.20	112.80	111.95	112.00
N3	C9	C20	116.09	118.71	128.14	126.99	117.40	127.57
N4	C9	C20	119.40	125.82	118.99	118.66	122.61	118.83
N4	C11	C12	106.28	105.66	106.30	105.61	105.97	105.96
N4	C11	C13	131.32	132.83	131.32	132.82	132.08	132.07
C12	C11	C13	122.39	121.51	122.38	121.57	121.95	121.98
N3	C12	C11	107.82	107.70	107.79	107.75	107.76	107.77
N3	C12	C16	131.51	131.48	131.52	131.47	131.50	131.50
C11	C12	C16	120.67	120.80	120.69	120.76	120.74	120.73
C11	C13	C14	115.84	117.81	115.83	117.74	116.83	116.79
C13	C14	C15	121.50	122.03	121.53	122.10	121.77	121.82
C14	C15	C16	122.96	119.93	122.91	119.92	121.45	121.42
C12	C16	C15	116.63	117.86	116.64	117.84	117.25	117.24
N5	C17	C18	114.73	111.16	114.78	111.12	112.95	112.95
C1	C18	C17	113.36	108.89	109.90	104.75	111.13	107.33
N5	C19	C20	124.75	110.70	124.79	110.68	117.73	117.74
C9	C20	C19	102.16	99.06	111.86	105.92	100.61	108.89

Table SI-1 4. MXAN best-fit results for the non-structural parameters

structure	overlap factor (%)	Fermi energy	broadening parameters			error (S^2)
			Γ_c (eV)	Γ(E)		
				E_s (eV)	A_s	
Cu(2-BB)(N3)	3.4	-1.88	2.22	25.16	9.69	0.30
Cu(2-BB)(2O) (**a**)	5.4	-1.05	2.35	16.52	11.91	0.22
Cu(2-BB)(O) (**a**)	6.3	-0.27	2.43	17.30	12.13	0.21
Cu(2-BB)(2O) (**b**)	4.3	- 0.95	2.30	16.99	14.23	0.21
Cu(2-BB)(O) (**b**)	4.7	- 0.45	2.41	17.88	14.60	0.21

The values of the error function (S^2) indicate that the agreement between the theoretical and experimental data is very good in the energy region chosen for the simulations. The values of Γ_c are reasonable considering that the core-hole lifetime width of copper is 1.55 eV.[8]

(**a**) and (**b**) refer to the best-fits from, respectively, the XRD data of the $[Cu(2\text{-}BB)(MeOH)(ClO_4)]^+$ and of the $[Cu(2\text{-}BB)(NO_2)]^+$ cations considered as starting models with five- and four-coordinated cores. *See text*.

Figure SI-1 1. Theoretical full MS cross-section calculations with the CONTINUUM code of the Cu K-edge absorption of the mononuclear complexes of the 2-BB ligand with different coordination geometries. Clusters of atoms corresponding to the entire cationic complexes have been considered. (a) $[Cu(2\text{-}BB)N_3]^+$ cation complex, (b) $[Cu(2\text{-}BB)(MeOH)(ClO_4)]^+$ cation complex, (c) $[Cu(2\text{-}BB)(NO_2)]^+$ cation complex. Reproduced from ref. 9.

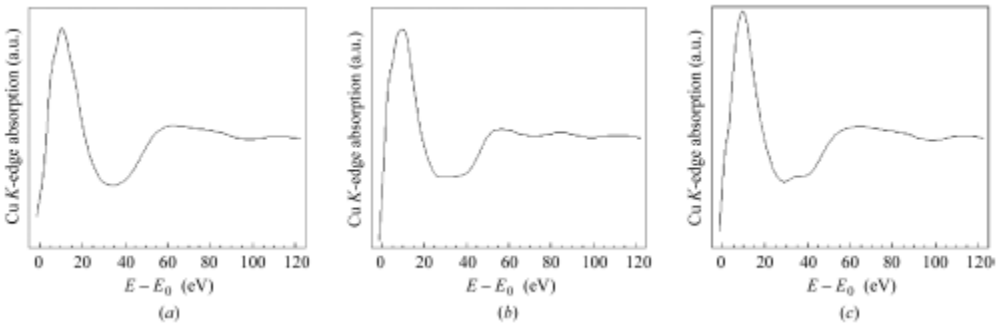

References SI-1

1 M. Benfatto and S. Della Longa, *J. Synchrotron Radiat*. 2001, **8**, 1087–1094.
2 M. Benfatto, S. Della Longa, and C. R.Natoli, *J. Synchrotron Radiat*. 2003, **10**, 51-57
3 C. R. Natoli, M. Benfatto, S. Della Longa and K. Hatada, *J. Synchrotron Radiat*. 2003, **10**, 26-42.
4 T. A. Tyson, K. O. Hodgson, C. R. Natoli and M. Benfatto, *Phys. Rev. B* 1992, 46, 5997-6019.
5 E. Clementi and C. Roetti, *Atom. Data Nucl. Data Tables* 1974, **14**, 177-478.
6 L. Hedin and B. I. Lundqvist, *J. Phys. C* 1971, **4**, 2064-2083.
7 L. Casella, O. Cargo, M. Gullotti, S. Doldi and M. Frassoni, *Inorg. Chem*. 1996, **35**, 1101-1113.
8 M. O. Krause and H. H: Oliver, *J. Phys. Chem. Ref. Data* 1979, **8**, 329-338.
9 E. Borghi and P. L. Solari, *J. Synchrotron Radiat.* 2005, **12**, 102-110.

Supporting Information
for

X-ray absorption spectroscopy quantitative analysis of biomimetic copper(II) complexes with tridentate nitrogen ligands mimicking the tris(imidazole) array of protein centres

Elena Borghi*[a] and Luigi Casella[b]

[a]Dipartimento di Chimica, Università di Roma "La Sapienza", Piazzale A. Moro 5, 00185 Roma, Italy and [b]Dipartimento di Chimica Generale, Università di Pavia, via Taramelli 12, 27100 Pavia, Italy

e.borghi@caspur.it and bioinorg@unipv.it

SI-2. EXAFS analysis in multiple-scattering (MS) formalism: the MS theoretical calculations considered to achieve a good fit of the experimental spectrum of the $[Cu(2\text{-}BB)(H_2O)_n](ClO_4)\cdot(H_2O)_{2-n}$ (n=1 or 2) complex in powder form

The EXAFS analysis has been performed using the GNXAS set of programs.[1-3] This code, which takes full account of the MS effects, is particularly suited for analyzing disordered systems and has been successfully applied to investigate biological or biological-related samples. The GNXAS program, given an atomic cluster [i.e. the model structure], finds all inequivalent absorbers, calculates ab-initio the associate signals and compares their sum to the experimental signal. The ability of the method in reproducing known structures in test cases has been amply documented in the literature. The theoretical signal is subsequently refined against the experimental signal in order to determine the structural parameters of the sample. With GNXAS, differently from other advanced analysis codes, starting from the model structure, the total theoretical EXAFS $\chi(k)$ signal is not decomposed as a sum of signals related to the number of scattering events [i.e. $\chi(2)$, $\chi(3)$, $\chi(4)$] but as a sum of signals related to the different two-body, three-body and four-body sub-geometries inside the system of atoms [i.e. $\gamma(2)$, $\gamma(3)$ and $\gamma(4)$]. The structural parameters associated with a generic n-body signals [i.e. the multiplicity N, the distances R, the angles θ, the dihedral angles ψ and their associated Debye Waller (DW) factors, σ^2] can be obtained with best fits [for more details see, for example, Di Cicco (2003)[4]].

Distinguishing the multiplicity of the n-body signals and taking into account the single and multiple scatterings coming from the n-atoms, the theoretical EXAFS signal is calculated as

$$\chi(k) = \sum \gamma(2) + \gamma(3) + \gamma(4)$$

In order to avoid signal proliferation in a fitting procedure it is essential to group the signals associated with the same n-atom configuration. This procedure is convenient to reduce the calculation parameters especially in the case of leading signals with comparable frequencies. A typical example is that of a structure with a first coordination shell and a second coordination shell. The second shell atom will be first shell of the first shell, therefore each second shell distance is also part of a triangle with an additional intermediate first shell atom. In this case the grouping procedure can combine the $\gamma(n)$ signals with different n values involving sub-clusters of the main n-atom configuration, considering the n-body signal $\eta(n)$ defined as

$$\eta(n) = \gamma(n) + \sum_{j=2}^{n-1} \gamma(j)$$

Thus, for a three-body configuration, the corresponding $\eta(3)$ signal consists of a three-body $\gamma(3)$ signal and a $\gamma(2)$ signal between the two more distant atoms ($\gamma_{LB}(2)$, LB=long-bond signal), [*i.e.* $\eta(3) = \gamma(3) + \gamma_{LB}(2)$]. An effective four-body $\eta(4)$ signal consists of a two-body long-bond signal, of a three body signals, and of a four-body signal, [*i.e.* $\eta(4) = \gamma(4) + \gamma(3) + \gamma_{LB}(2)$].

The refined MS results, [5, 6] including the previously unpublished values of the angular parameters, for the hypothetical $[Cu(2\text{-}BB)(H_2O)_2](ClO_4)$ complex in the $[Cu(2\text{-}BB)(H_2O)_n](ClO_4)\cdot(H_2O)_{2-n}$ (n=1 or 2) powder form, obtained by taking as a starting structure the XRD data of the $[Cu(2\text{-}BB)(MeOH)(ClO_4)](ClO_4)$ complex,[7] are presented in Table SI-2 1.

Figure SI-2 1 shows the crystal structure and the related 28-atoms cluster used in the fit. Figure SI-2 2 shows the n-body scattering paths considered for the EXAFS fit. The results of the fit for the EXAFS signal, including details of the different theoretical signals used, are shown in Figure SI-2 3.

Figure SI-2 1. Crystal structure and related cluster used as model for the EXAFS fit

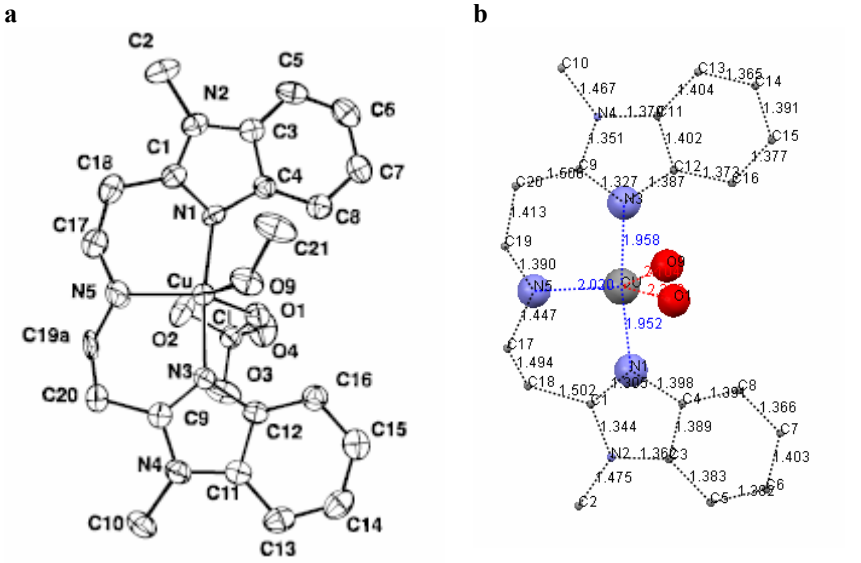

a Crystal structure of the $[Cu(2BB)(MeOH)(ClO4)]^{+}$ cation, reproduced from ref.7.

b A 28-atoms cluster was used in the fit. The model includes atoms within a distance of ~5.7 Å from the absorbing Cu centre, and uses in equatorial position only the perchlorate oxygen atom O1 and the methanol oxygen atom O9.

Figure SI-2 2. The n-body scattering paths considered for the fit of the EXAFS spectrum of the $[Cu(2\text{-}BB)(H_2O)_2]^{+}$ cation

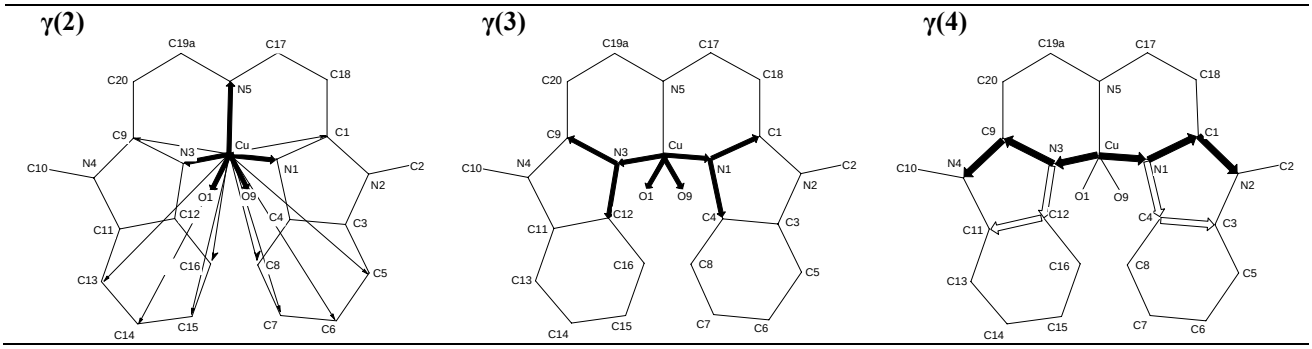

Figure SI-2 3. Detail of the theoretical signals considered for the final fit of the spectrum of the $[Cu(2\text{-}BB)(H_2O)_2]^+$ cation

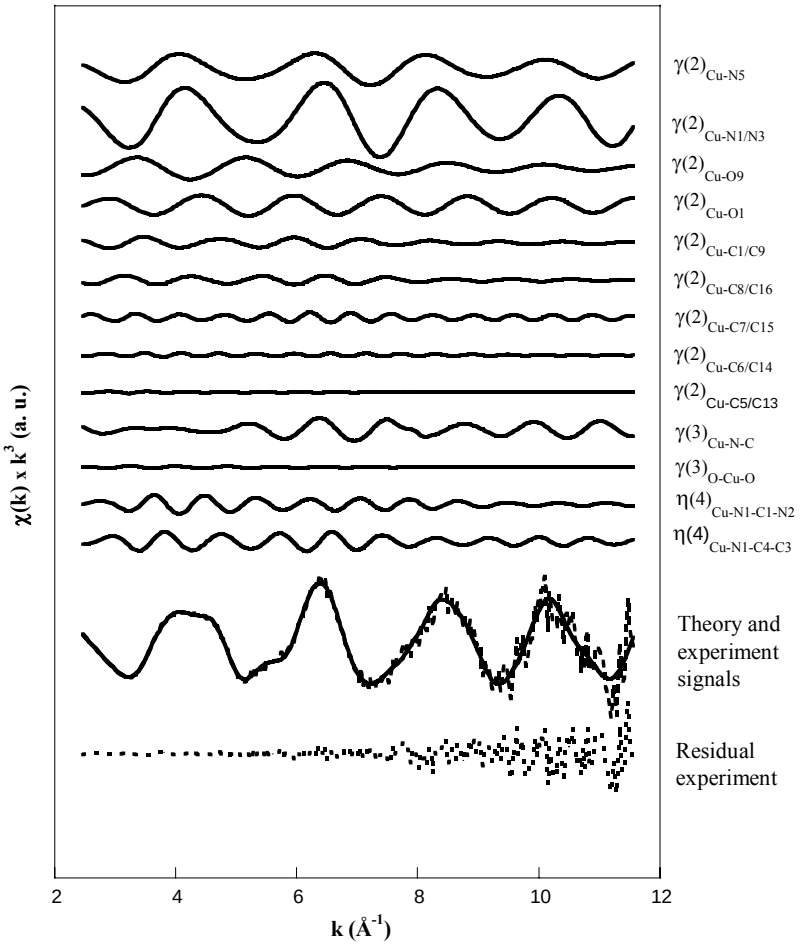

Table SI-2 1. Results obtained for the hypothetical $[Cu(2\text{-}BB)(H_2O)_2]^+$ cation in the $[Cu(2\text{-}BB)(H_2O)_n](ClO_4)\cdot(H_2O)_{2-n}$ powdered complex starting from the structure of $[Cu(2BB)(MeOH)(ClO_4)]^+$ cation

n-body scattering paths inside the cluster of 28 atoms					
n-body Signal	**Structural parameter associated**	**Structural feature x multiplicity**	Distance (Å) or angle (°)	**σ_{dist}^2(Å^2) or σ_{ang}^2 (°^{2})**	**XRD Distance (Å) or angle (°)**
Two-body scattering paths Cu(o)–N/O/C(i)					
γ(2)	**Ro,i**	Cu–N5 x 1	2.01	0.002	2.02
		Cu–N1/N3 x 2	1.97	0.001	1.96
		Cu–O9 x 1	2.30	0.006	2.11
		Cu–O1 x 1	2.58	0.001	2.33
		Cu–C1/C9 x 2	3.19	0.009	2.92
		Cu–C8/C16 x 2	3.45	0.008	3.38
		Cu–C7/C15 x 2	5.07	0.003	4.90
		Cu–C6/C14 x 2	5.75	0.01	5.42
		Cu–C5/C13 x 2	5.50	0.01	5.62
Three-body scattering paths inside imidazole: Cu(o)–N1(i)–C1/C4(j) and Cu(o)–N3(i)–C9/C12(j)					
	Ro,i	Cu–N1/N3 x 2	1.97	0.001	2.02
	Ri,j	N1–C1/C4 ; N3–C9/C12 x 4	1.30	0.001	1.30
	θoij	Cu–N1–C1/C4 ; Cu–N3–C9/C12 x 4	126.1	2.35	125.7
η(3)= γ(3)+γ_{LB}(2)	**Ro,j**	Cu–C1/C4 ; Cu–C9/C12 x 4	2.963	0.006	2.92
Three-body scattering path: O(i)–Cu(o)–O(j)					
γ(3)	**Ro,i**	Cu–O9 x 1	2.30	0.001	2.10
	Ri,j	Cu–O1 x 1	2.58	0.006	2.33
	θoij	O9–Cu–O1 x 1	127.0	1.07	119.1
Four-body scattering paths inside imidazole: Cu(o)–N1(i)–C1(j)–N2(k) and Cu(o)–N3(i)–C9(j)–N4(k)					
γ(4)	**Ro,i**	Cu–N1/N3 x 2	1.97	0.001	1.96
	Ri,j	N1/N3–C1/C9 x 2	1.30	0.001	1.31
	θoij	Cu–N1/N3–C1/C9 x 2	126.1	2.35	125.7
	Rj,k	C1/C9–N2/N4 x2	1.35	0.001	1.36
	φijk	N1/N3–C1/C9–N2/N4 x 2	109.9	16.43	110.4
	Ψ (Ri,j)		170.6	15.1	170.6
η(4)=γ(4)+γ_{LB}(3)	**Ro,k**	Cu–N2/N4 x 2	4.10	0.006	4.12
Four-body scattering paths inside imidazole: Cu(o)–N1(i)–C4(j)–C3(k) and Cu(o)–N3(i)–C12(j)–C11(k)					
γ(4)	**Ro,i**	Cu–N1/N3 x 2	1.97	0.001	1.96
	Ri,j	N1/N3–C4/C12 x2	1.44	0.001	1.40
	θoij	Cu–N1/N3–C4/C12 x2	128.5	1.047	128.5
	Rj,k	C4/C12–C3/C11 x 2	1.38	0.003	1.39
	φijk	N1/N3–C4/C12–C3/C11 x2	109.9	16.43	107.8
	ψ (Ri,j)		170.6	15.1	171.4
η(4)= γ(4)+ γ_{LB}(3)	**Ro,k**	Cu–C3/C11 x 2	4.22	0.016	4.19
Residual, experiment 0.806 x 10^{-6}					

To test the GNXAS method for the analysis of such biomimetic models, the first step has been to consider the spectrum of the $[Cu(2\text{-}BB)(N_3)](ClO_4)$ complex in powder form, to compare the best fit results of the EXAFS region with the crystallographic data [7]. To avoid radiation damage the spectrum of this sample has been collected with an average of only three single scans. The EXAFS curve is resulting noisy and with a short k-range ($k \leq 8 Å^{-1}$) of usable data. The calculated expected value of the residual [2, 3] for this spectrum is elevated ($R_{th} = 0.92458 \times 10^{-6}$) and comparable to the best fit value of the residual ($R_{exp} = 0.107 \times 10^{-5}$). Such an experimental difficulty reduces the goodness of the fit.

The refined MS results,[5,6] including the previously unpublished values of the angular parameters, for the $[Cu(2\text{-}BB)(N_3)](ClO_4)$ complex in powder form, obtained by taking as a starting structure the XRD data of the $[Cu(2\text{-}BB)(N_3)](ClO_4)$ complex, [7] are presented in Table SI-2 2.

Figure SI-2 4 shows the crystal structure and the related 29-atoms cluster used in the fit. Figure SI-2 5 shows the n-body scattering paths considered for the EXAFS fit. The results of the fit for the EXAFS signal, including details of the different theoretical signals used, are shown in Figure SI-2 6.

Figure SI-2 4. Crystal structure and related cluster used as model for the EXAFS fit

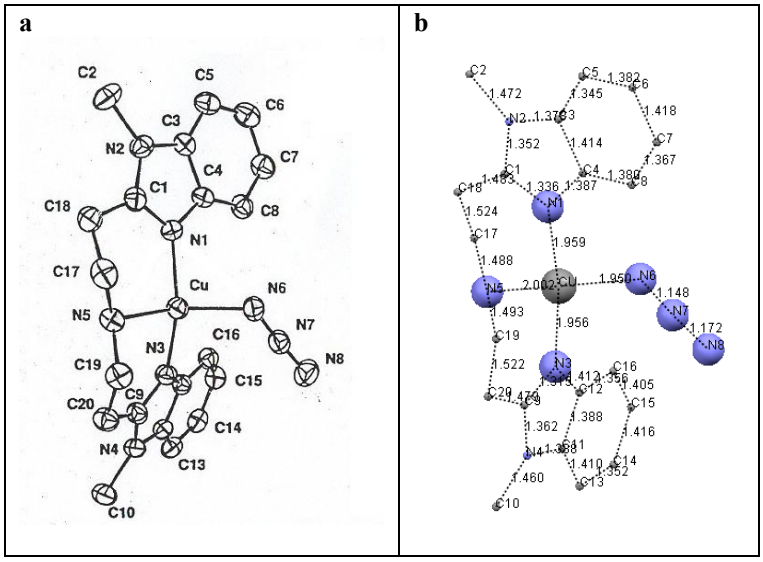

a View of the $[Cu(2\text{-}BB)(N_3)]^+$ cation in the $[Cu(2\text{-}BB)(N_3)]$ (ClO_4) crystal reproduced from ref.7. **b** A 29-atoms cluster was used in the fit. The model includes atoms within a distance of ~5.4 Å from the absorbing Cu centre.

Figure SI-2 5. The n-body scattering paths considered for the fit of the EXAFS spectrum of the $[Cu(2\text{-}BB)(N_3)]^+$ cation of the complex in powder form

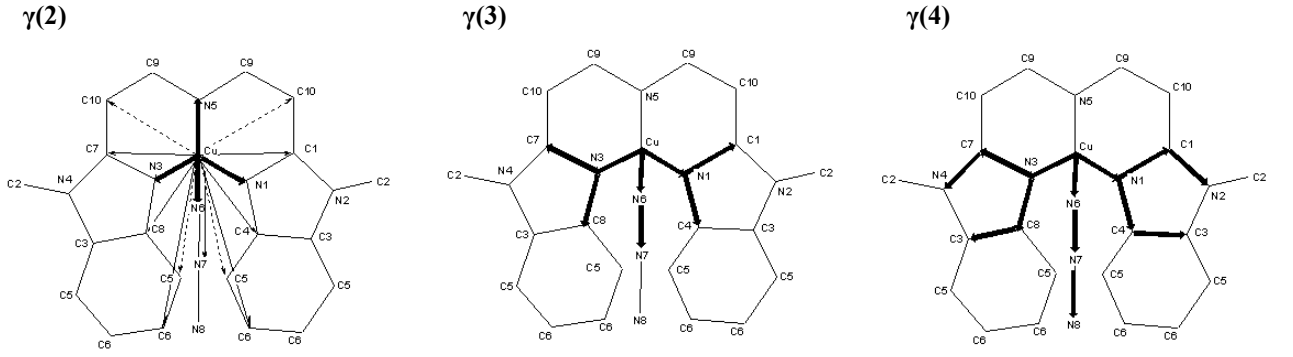

Figure SI-2 6. Detail of the theoretical signals considered for the final fit of the spectrum of the $[Cu(2\text{-}BB)(N_3)]^+$ cation of the complex in powder form

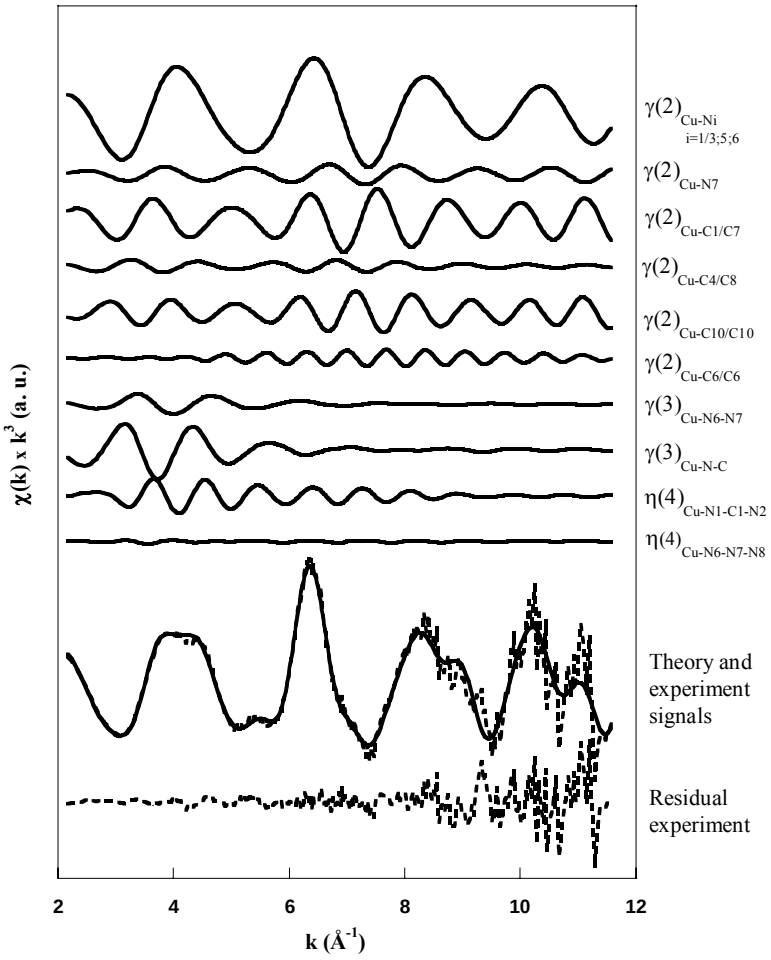

Table SI-2 2. Results obtained for the $[Cu(2\text{-}BB)(N_3)]^+$ cation of the complex in powder form starting from the structure of the $[Cu(2\text{-}BB)(N_3)]^+$ cation in the $[Cu(2\text{-}BB)(N_3)](ClO_4)$ crystal

n-body scattering paths inside the cluster of 29 atoms					
n-body Signal	**Structural parameter associated**	**Structural feature x multiplicity**	**Distance (Å) or angle (°)**	**σ_{dist}^2(Å^2) or σ_{ang}^2 (°^{2})**	**XRD Distance (Å) or angle (°)**
Two-body scattering paths Cu(o)–N/C(i)					
γ(2)	**Ro,i**	Cu–N5 x 1			2.00
		Cu–N1/N3 x 2	1.96	0.002	1.96
		Cu–N6 x 1			1.95
		Cu–N7 x 1	2.75	0.007	2.79
		Cu–C1/C7 x 2	2.96	0.003	2.93
		Cu–C4/C8 x 2	3.22	0.009	3.00
		Cu–C5/C10 x 4	3.56	0.001	3.37
		Cu–C6 x 2	4.94	0.001	4.90
Three-body scattering paths inside imidazole: Cu(o)–N1(i)–C1/C4(j) and Cu(o)–N3(i)–C7/C8(j)					
	Ro,i	Cu–N1/N3 x 2	1.96	**0.002**	1.96
	Ri,j	N1–C1/C4 ; N3–C7/C8 x 4	1.35	0.003	1.32
	θoij	Cu–N1–C1/C4 ; Cu–N3–C7/C8 x 4	126.6	24.18	125.7
η(3)= γ(3)+γ_{LB}(2)	**Ro,j**	Cu–C1/C4 ; Cu–C7/C8 x 4	2.78	0.008	2.86
Three-body scattering path: Cu(o)–N6(i)–N7(j)					
	Ro,i	Cu–N6 x 1	1.96	0.002	1.95
	Ri,j	N6–N7 x 1	1.11	0.001	1.15
	θoij	Cu–N6–N7 x 1	125.0	15.21	126.3
η(3)= γ(3)+γ_{LB}(2)	**Ro,j**	Cu–N7 x 1	2.78	0.006	2.79
Four-body scattering paths inside imidazole: Cu(o)–N1(i)–C1(j)–N2(k) and Cu(o)–N3(i)–C7(j)–N4(k)					
γ(4)	**Ro,i**	Cu–N1/N3 x 2	1.96	0.002	1.96
	Ri,j	N1/N3–C1/C7 x 2	1.34	0.004	1.34
	θoij	Cu–N1/N3–C1/C7 x 2	127.8	15.21	125.7
	Rj,k	C1/C7–N2/N4 x2	1.30	0.001	1.35
	φijk	N1/N3–C1/C7–N2/N4 x 2	112.7	23.33	110.6
	ψ (Ri,j)		182.4	1.3	178.1
η(4)=γ(4)+γ_{LB}(3)	**Ro,k**	Cu–N2/N4 x 2	4.10	0.006	4.12
Four-body scattering paths inside azide: Cu(o)–N6(i)–N7(j)–N8(k)					
γ(4)	**Ro,i**	Cu–N6 x 1	1.96	0.002	1.95
	Ri,j	N6–N7 x 1	1.11	0.003	1.15
	θoij	Cu–N6–N7 x 1	127.5	15.21	126.3
	Rj,k	N7–N8 x 1	1.11	0.003	1.17
	φijk	N6–N7–N8 x 1	176.3	1.0	176.3
	ψ (Ri,j)		163.3	15.16	164.4
η(4)= γ(4)+ γ_{LB}(3)	**Ro,k**	Cu–N8 x 1	4.22	0.016	4.19
Residual, experiment 0.107x 10^{-5}					

References SI-2

1 A. Filipponi, A. Di Cicco and C. R. Natoli, *Phys. Rev. B* 1995, **52**, 15122-15134.
2 A. Filipponi and A.Di Cicco, *Phys. Rev. B* 1995, **52**, 15135-15149.
3 A. Filipponi and A. Di Cicco, *Task Q*. 2000, **4**, 575- 669.
4 A. Di Cicco, *J. Synchrotron Rad*. 2003, **10**, 46-50.
5 E. Borghi, P. L: Solari, M. Beltramini, l. Bubacco, P. Di Muro and B. Salvato, *Biophys. J*. 2002, **82**, 3254–3268.
6 M. Friello and E. Borghi, http://www.circmsb.uniba.it/ 2003
7 L. Casella, O. Cargo, M. Gullotti, S. Doldi and M. Frassoni, *Inorg. Chem*. 1996, **35**, 1101-1113